Journal of Engineering Mathematics **33:** 113–128, 1998.

Radial stagnation flow on a rotating circular cylinder with uniform transpiration

G. M. CUNNING[1], A. M. J. DAVIS[2] and P. D. WEIDMAN[3]*
[1]*Research Applications Program, NCAR, Boulder, CO 80307 USA*
[2]*Department of Mathematics, University of Alabama, Tuscaloosa, AL 35487 USA*
[3]*Laboratoire d'Hydrodynamique, Ecole Polytechnique, 91128 Palaiseau, France*

Received 28 May 1996; accepted in revised form 1 July 1997

Abstract. Radial stagnation flow of strain rate k impinging on a cylinder with uniform transpiration U_0 and rotating at constant angular velocity ω is investigated. An exact reduction of the Navier-Stokes equations to a primary nonlinear equation for the meridional flow similar to that found by Wang and a secondary linear equation for the azimuthal flow is obtained. The governing parameters are the stagnation-flow Reynolds number $R = ka^2/2\nu$, the dimensionless transpiration $S = U_0/ka$, and the dimensionless rotation rate $\Omega = \omega/k$, where a is the cylinder radius and ν is the kinematic viscosity of the fluid. The boundary-value problem is solved by numerical integration and by asymptotic analysis in certain limits. The results are succinctly summarized in plots of the axial and azimuthal shear-stress parameters as functions of R and S. Sample velocity profiles, meridional streamfunction plots, and projections of particle paths for both suction and blowing are given. An interesting double-layer structure in the azimuthal velocity profile, consisting of a removed free shear layer connected to a wall boundary layer, is observed at large values of blowing. This feature is consistent with results obtained from the asymptotic analysis.

Key words: stagnation flow, rotation, suction, blow-off, exact solution

1. Introduction

We investigate the nature of axisymmetric radial stagnation flow on a rotating circular cylinder with uniform transpiration, including both suction and blowing. This study extends the work of Wang [1], who first reported the solution for steady radial stagnation flow impinging on a stationary cylinder with impermeable walls. Both Wang's solution and the results presented here represent exact steady-flow solutions of the Navier-Stokes equations. A review of such exact solutions of the Navier-Stokes equations has been given by Wang [2]. In that review, and elsewhere, one finds papers by Gorla [3, 4, 5] dealing with steady and unsteady flow extensions of the radial stagnation flow problem, and also several other papers by Gorla that consider the radial stagnation flow of non-Newtonian fluids. The effects of cylinder rotation and wall suction, perhaps of interest in certain special manufacturing processes, have not yet been considered.

The classical two-dimensional Hiemenz [6] and three-dimensional Homann [7] stagnation flows describe situations where fluid impinges normally onto a flat surface and spreads out bidirectionally or radially along the surface, away from a single stagnation point. The stagnation flow depicted in Figure 1, on the other hand, consists of a radially inward flowing stream impinging normally on a cylindrical surface and spreading out axially away from a stagnation circle. While Hiemenz and Homann stagnation-point flows represent self-similar

* Permanent address: Department of Mechanical Engineering, Campus Box 427, University of Colorado, Boulder, CO 80309 USA

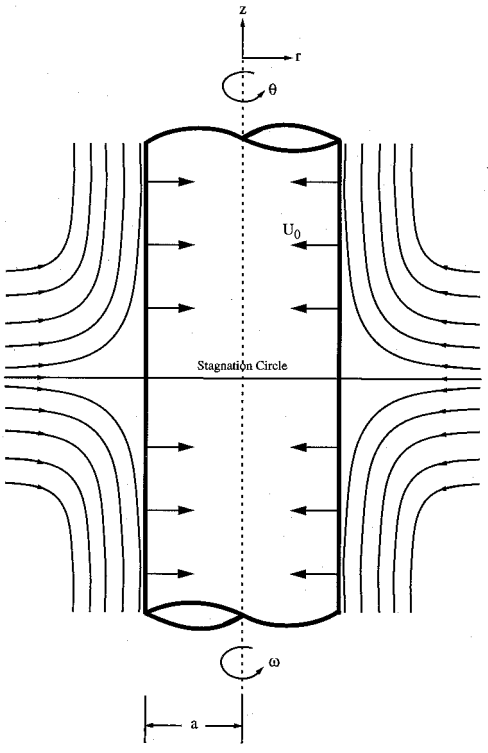

Figure 1. Schematic diagram of a rotating cylinder with uniform transpiration under radial stagnation flow. Also shown is the fixed cylindrical coordinate system (r, θ, z).

reductions of the Navier-Stokes equations, radial stagnation flow does not. This is due to inherent curvature effects that cannot be scaled out of the problem [1].

The presentation is as follows. The governing equations of motion and their reduction to a coupled set of ordinary differential equations are given in Section 2 along with a discussion of the numerical solution procedure. Certain asymptotic results for large values of suction and blowing Reynolds numbers are presented in Section 3. The numerical solutions given in Section 4 are compared with the asymptotic behaviours and boundary-layer structures found in Section 3 in the large-suction and large-blowing limits. A discussion of results and concluding remarks are given in Section 5.

2. Problem formulation and solution procedure

Flow is considered in cylindrical coordinates (r, θ, z) with associated unit vectors $(\mathbf{e}_r, \mathbf{e}_\theta, \mathbf{e}_z)$ and velocity components (u, v, w). A cylinder with radius a having infinite axial extent is centered on $r = 0$. The cylinder rotates at constant angular rate ω, and uniform normal transpiration U_0 at the cylinder surface may occur. An external axisymmetric radial stagnation flow characterized by strain rate k impinges on the cylinder. The flow configuration is depicted in Figure 1 where it may be noted that $U_0 > 0$ corresponds to suction into the cylinder.

The steady flow is governed by the equation of continuity and the viscous incompressible Navier-Stokes equations

$$\boldsymbol{\nabla} \cdot \boldsymbol{u} = 0, \tag{1}$$

$$(\boldsymbol{u}\cdot\boldsymbol{\nabla})\boldsymbol{u} = -\frac{1}{\rho}\boldsymbol{\nabla}p + \nu\nabla^2\boldsymbol{u}, \tag{2}$$

where p, ρ, and ν are the fluid pressure, density, and kinematic viscosity. As $r \to \infty$, the viscous flow approaches, in a manner analogous to the Hiemenz flow, the potential stagnation flow field given by

$$u = -k\left(r - \frac{a^2}{r}\right) - U_0\frac{a}{r}, \qquad \lim_{r\to\infty} rv = 0, \qquad w = 2kz, \tag{3}$$

$$p = p_0 - \frac{\rho k^2}{2}\left[4z^2 + \left(r + \left\{\frac{U_0}{k} - a\right\}\frac{a}{r}\right)^2\right], \tag{4}$$

in which p_0 is the stagnation pressure and the case $U_0 = 0$ is that discussed by Wang [1]. The presence of the stagnation flow allows the condition of zero circulation at infinity to be imposed on the swirl velocity.

A reduction of the Navier-Stokes equations is obtained by the following coordinate separation of the velocity field

$$u = -k\frac{a}{\sqrt{\eta}}f(\eta), \qquad v = \omega\frac{a}{\sqrt{\eta}}g(\eta), \qquad w = 2kf'(\eta)z, \qquad p = \rho k^2a^2P, \tag{5}$$

where $\eta = (r/a)^2$ is the dimensionless radial variable. The solution form (5) satisfies (1) exactly and its insertion into (2) yields a primary equation for f, an equation for g slaved to f, and an expression for the pressure, *viz.*

$$\eta f''' + f'' + R[1 - (f')^2 + ff''] = 0, \tag{6}$$

$$\eta g'' + Rfg' = 0, \tag{7}$$

$$P = P_0 - \left[\frac{f^2}{2\eta} + \frac{1}{R}f' + 2\left(\frac{z}{a}\right)^2 - \frac{\Omega^2}{2}\int_1^\eta \frac{g^2(\xi)}{\xi^2}\,\mathrm{d}\xi\right], \tag{8}$$

in which R is a Reynolds number. On the surface of the cylinder, the axial velocity satisfies the no-slip boundary condition, while the radial and azimuthal velocities are the imposed transpiration rate U_0 and cylinder rotation speed ωa, respectively. The solution should tend towards a displaced form of the inviscid solution (3) and (4) as $\eta \to \infty$. Thus (6)–(8) must satisfy the boundary conditions

$$f(1) = S, \qquad f'(1) = 0, \qquad f'(\infty) = 1, \tag{9}$$

$$g(1) = 1, \qquad g(\infty) = 0, \tag{10}$$

in which the vanishing of g at infinity will be seen to be necessary. The flow depends on the stagnation-flow Reynolds number R, the dimensionless wall-transpiration rate S, and the dimensionless cylinder rotation rate Ω, where

$$R = \frac{ka^2}{2\nu}, \qquad S = \frac{U_0}{ka}, \qquad \Omega = \frac{\omega}{k}. \tag{11}$$

Since U_0 is the radially inward transpiration velocity at $r = a$, $S > 0$ corresponds to suction. Observe also that Ω is a free parameter, since it does not appear in the boundary-value problem described by (6)–(10); however, if $\Omega = 0$ the equation for $g(\eta)$ is superfluous. Solutions of the boundary-value problem represent an exact solution of the full Navier-Stokes equations for arbitrary positive values of R and for arbitrary positive and negative values of S and Ω. The shear stress at the cylinder surface is calculated from the equation

$$\boldsymbol{\tau} = \mu \left[r \frac{\partial}{\partial r} \left(\frac{v}{r} \right) \mathbf{e}_\theta + \frac{\partial w}{\partial r} \mathbf{e}_z \right]_{r=1} = 2k\mu \left[\Omega \{ g'(1) - 1 \} \mathbf{e}_\theta + 2 \left(\frac{z}{a} \right) f''(1) \mathbf{e}_z \right], \tag{12}$$

where $\mu = \rho\nu$ is the dynamic fluid viscosity. Thus the axial and azimuthal shear-stress components are proportional to $f''(1)$ and $[g'(1) - 1]$, respectively.

Solutions for limiting cases have been reported in the literature. The case $\Omega = S = 0$ corresponds to radial stagnation flow on a cylinder studied by Wang [1]; he presented representative numerical solutions at $R = 0.1, 1, 10$. When the radial stagnation flow is absent, found in the limit $|S| \to \infty$ with the suction Reynolds number

$$RS = U_0 a / 2\nu \tag{13}$$

remaining finite, motion is driven by the cylinder rotating in a quiescent viscous fluid with uniform boundary transpiration. This flow has solution (*cf.* Sherman [8, p. 159])

$$f = S, \qquad g = 1 + \frac{B}{\omega a} (\eta^{1-RS} - 1), \qquad w = 0, \tag{14}$$

where B is an arbitrary velocity. This yields

$$g = 1 \quad (RS < 1), \qquad g = \eta^{1-RS} \quad (RS > 1), \tag{15}$$

after relaxing, for $RS < 1$, the requirement that the circulation tends to zero as η goes to infinity. The shear stress for this case is

$$\boldsymbol{\tau} = -2\mu \max(1, RS) \omega \, \mathbf{e}_\theta. \tag{16}$$

The solution of (7) for g', namely

$$g'(\eta) = g'(1) \exp \left[-R \int^\eta \frac{f(\xi)}{\xi} \, \mathrm{d}\xi \right], \tag{17}$$

demonstrates that g is determined from f; in particular, the condition $f'(\infty) = 1$ in (9) implies that g' decays exponentially when $R \neq 0$, and hence zero circulation at infinity must be imposed.

In the present investigation, we seek exact solutions where all three physical effects of cylinder rotation, wall transpiration, and radial stagnation flow come into play. For plotting purposes it is convenient to introduce a dimensionless Stokes stream function $\hat{\psi}$ defined by

$$\hat{\psi} = \frac{\psi}{ka^3} = f(\eta) \left(\frac{z}{a} \right), \tag{18}$$

where dimensional velocities (u, v) are given by $(-1/r\partial\psi/\partial z, 1/r\partial\psi/\partial r)$. Note that $\hat{\psi} = 0$ corresponds to the streamline passing through the symmetry plane $z = 0$.

The boundary-value problem (6)–(10) is resolved numerically by means of a modified nonlinear shooting method. A stiff-equation solver based on the Bulirsch-Stoer method is employed, and the boundary values are iterated by means of the secant method. The differential-equation solver is taken from the FORTRAN programs listed by Press, *et al.* [9, pp. 718–739]. The calculations took place on a UNIX-based workstation, using double-precision arithmetic.

The basic nonlinear shooting method was modified so that solutions could be obtained in regions where the governing parameters R and S made the differential equations unusually stiff or sensitive. For prescribed values of R and S, the equations are solved as an initial-value problem, using guesses for $f''(1)$ and $g'(1)$, and integrated to sufficiently large values of η. The solutions are iterated based on updated values of $f''(1)$ and $g'(1)$. Updates are determined by a secant method on the far field conditions (9) and (10) at large η. Another level of iteration is utilized to march the solutions to large η.

3. Asymptotic analysis

Since the boundary-value problem is governed by R and S, it is desirable to determine the asymptotic nature of solutions for large values of these parameters where the integrations become increasingly difficult. The problem for $S = 0$ and $R \gg 1$ was discussed by Wang [1]. He showed that a transformation of dependent and independent variables can be made that leads to the planar Hiemenz [6] problem as a first approximation for $R \to \infty$ with an error $O(R^{-1/2})$. Since no analytic solution of the nonlinear Hiemenz equation is available, the asymptotic analysis for zero transpiration is solvable only with the aid of numerical integration. However, when suction or blowing is present, we show below that the leading-order behavior of the shear stress parameters may be obtained for large suction/blowing if $R = O(1)$, and for large Reynolds number if $S = O(1)$, *i.e.* for large positive or negative values of the suction Reynolds number defined by (13).

3.1. Suction asymptotics

With large suction, $S \gg 1$, the flow is fully viscous in the vicinity of the cylinder and we introduce appropriate boundary-layer variables by writing

$$\zeta = RS(\eta - 1), \qquad f(\eta) = S + H(\zeta)/RS. \tag{19}$$

Substitution in Equations (6) and (9) and identification of the dominant terms, at large RS, leads to the approximate boundary-value problem governing the meridional flow

$$H''' + H'' = 0, \qquad H(0) = H'(0) = 0, \qquad H'(\infty) = 1. \tag{20}$$

The solution $H = \zeta - 1 + \mathrm{e}^{-\zeta}$ yields, on substitution in (19), an $f(\eta)$ uniformly valid in η correct to $O(1/RS)$, *viz.*

$$f(\eta) = S + (\eta - 1) - \frac{1}{RS}\left[1 - \mathrm{e}^{-RS(\eta-1)}\right]. \tag{21}$$

The asymptotic suction profile and the leading-order wall-shear-stress parameter, used for comparison with numerical solutions in Section 4, are given by

$$f'(\eta) = 1 - \mathrm{e}^{-RS(\eta-1)}, \qquad f''(1) \sim RS \quad (RS \gg 1). \tag{22}$$

The above analysis follows that of Pretsch [10], as outlined in Rosenhead [11, p. 252], and demonstrates that, for large values of S, $f \sim S$, and therefore the terms $(1 - f'^2)$ can be neglected relative to ff'' in (6).

The leading-order behavior of (21), namely $f \sim S$ for $RS \gg 1$, reduces Equation (7) governing the azimuthal motion to the equidimensional equation $\eta g'' + RSg' = 0$. The asymptotic solution of (7) satisfying boundary conditions (10) and the shear stress due to the azimuthal flow is then

$$g(\eta) = \eta^{1-RS} \sim \mathrm{e}^{-RS(\eta-1)}, \qquad g'(1) - 1 \sim -RS \quad (RS \gg 1). \tag{23}$$

Note that the e-folding scale $(RS)^{-1}$ of g demonstrates that the azimuthal velocity is confined to a layer of thickness $O(\nu/U_0)$ adjacent to the cylinder [*cf.* Equation (13)].

3.2. Blowing aysmptotics

We start from the premise that for sufficiently strong blowing, there is a region near the cylinder wall where f''', which measures the streamline curvature, is negligible. Then (6) reduces to the second-order nonlinear equation

$$f'' + R(1 - f'^2 + ff'') = 0, \tag{24}$$

which has the two-parameter family of solutions

$$f(\eta) = -\frac{1}{R} - C\,\cos\left(\frac{\eta - \eta_0}{C}\right). \tag{25}$$

We can satisfy the wall conditions in (9) by setting $\eta_0 = 1$ and $C = |S| - R^{-1}$ to obtain

$$f(\eta) = -\frac{1}{R} - \left(|S| - \frac{1}{R}\right)\,\cos\left(\frac{\eta - 1}{|S| - R^{-1}}\right), \tag{26}$$

for values of η up to $O(|S|)$. This is the scale of the inviscid solution, given by (21) with $(RS)^{-1} = 0$, and corresponds, according to (11), to radii of order $(|U_0|a/k)^{1/2}$. The axial shear-stress parameter in this limit is given by

$$f''(1) \sim \left(|S| - \frac{1}{R}\right)^{-1} \quad (R|S| \gg 1). \tag{27}$$

The leading two terms of this result can be formally established if we write

$$\xi = (\eta - 1)/|S|, \qquad f(\eta) = |S|F(\xi) \tag{28}$$

in (6) to obtain

$$1 - F'^2 + FF'' + \frac{1}{R|S|}\left[\left(\frac{1}{|S|} + \xi\right)F''' + F''\right] = 0. \tag{29}$$

The first two terms of the expansion

$$F = F_0 + \frac{1}{R|S|}F_1 + \cdots \tag{30}$$

are governed, according to (29) and (9), by

$$1 - F_0'^2 + F_0F_0'' = 0, \tag{31}$$

$$F_1''F_0 - 2F_0'F_1' + F_1F_0'' + \xi F_0''' + F_0'' = 0, \tag{32}$$

$$F_0(0) = -1, \qquad F_0'(0) = 0; \qquad F_1(0) = F_1'(0) = 0. \tag{33}$$

Hence $F_0 = -\cos\xi$ and the solution for F_1 is facilitated by noting that $F_0' = \sin\xi$ is a homogeneous solution of the equation for F_1. However, the wall-stress contribution is available, since F_0 is known, without solving Equation (32) which yields directly, with the aid of (33), that $F_1''(0) = 1$. Hence, from (28) and (30)

$$f''(1) = |S|^{-1}F''(0) \sim \frac{1}{|S|}\left[1 + \frac{1}{R|S|}\right] \quad (R|S| \gg 1), \tag{34}$$

in agreement with (27).

The condition (9) at infinity is satisfied by

$$f = -|S| + \eta - D^2, \tag{35}$$

which is a solution of (6), and a numerical integration of this third-order differential equation is required to connect (26) and (35) with appropriate matching. Note that, if the term $\eta f'''$ were absent from (6), then an exact solution would be available, since (26) can be smoothly matched to (35) at $\eta = 1 + \pi(|S| - R^{-1})/2$ by setting

$$D^2 = \left(|S| - \frac{1}{R}\right)\left(\frac{\pi}{2} - 1\right) + 1. \tag{36}$$

The scaling for the outer solution is given by (28). We need to match $F_0 = \cos\xi$ with the linear function $\xi +$ const., both of which are solutions of (31). This can be achieved at $\xi = \pi/2$ by setting the constant equal to $-\pi/2$, in agreement with (35) and (36).

We now turn to Equation (7) which is essentially solved by (17). Thus, g' is exponentially increasing or decreasing with η according as f is less than or greater than zero, respectively. When $f(\eta)$ is large and negative, as happens in a region adjacent to the cylinder, only the constant solution satisfying the wall boundary condition in (10) is admissible yielding

$$g(\eta) = 1, g'(1) - 1 = -1 \qquad (R|S| \gg 1). \tag{37}$$

When $f(\eta)$ is large and positive, as happens when η is sufficiently large, the decaying solution for $g(\eta)$ is selected, as required by the zero circulation condition in (10). The transition occurs in the interval containing the turning point in the differential equation (7) and becomes more abrupt as $|S|$ increases, as found numerically.

Suppose η_c is such that $f(\eta_c) = 0$. Then $f'(\eta_c) \cong 1$ and hence, near $\eta = \eta_c$,

$$f \sim \eta - \eta_c \quad (R|S| \gg 1). \tag{38}$$

Equation (7) is then approximated by

$$g'' \sim -R\left(\frac{\eta - \eta_c}{\eta_c}\right) g', \tag{39}$$

which yields the particular solution

$$g = \frac{1}{2}\left\{1 - \text{erf}\left[\sqrt{\frac{R}{2\eta_c}}(\eta - \eta_c)\right]\right\} + O\left[\frac{1}{\sqrt{R|S|}}\right]. \tag{40}$$

The exponential decay in $g(\eta)$ is rapid when $R|S| \gg 1$ because η_c is $O(|S|)$. So $g(\eta)$ changes from $1 + O[(R|S|)^{-1/2}]$ to $O[(R|S|)^{-1/2}]$ in an interval of width $O[(R|S|)^{-1/2}]$, centered at $\eta = \eta_c$. The subsequent decay of g to zero approximates a multiple of $\eta^{R\eta_c}\,\mathrm{e}^{-R(\eta-\eta_c)}$ as $\eta \to \infty$. The interesting behavior suggested above will be apparent in the numerical solutions for blowing at large $R|S|$ to be presented in Section 4.

4. Presentation of results

In this section the results of the numerical integrations are presented. The shear-stress parameters plotted over the solution space (R, S) given in Section 4.1 are compared with the asymptotic results for suction, valid for $RS \gg 1$, and blowing, valid for $R|S| \gg 1$. Sample boundary-layer velocity profiles are given in Section 4.2 and their convergence to the uniformly valid asymptotic suction profiles is displayed. Meridional streamline and projected pathline plots exhibiting the three-dimensional nature of the flow are presented in Section 4.3.

The numerical integrations have been carried out over as wide a range of R and S as possible. However, the solution space is limited by the stiffness (sensitivity) of the differential equations. Experimentation showed that equation stiffness increased in proportion to $R|S|$ for S both positive and negative. Thus, at low values of R, solutions were obtained over a relatively wide range of $|S|$ values, and *vice versa*.

4.1. Shear-stress parameters

The shear stress on the surface of the rotating cylinder in the presence of radial stagnation flow with boundary transpiration is calculated from Equation (12) and their plots over the solution space of R and S provide a succinct summary of the numerical results. In each figure the solid lines connect numerically computed points, while the dashed lines correspond to one of the asymptotic results determined in Section 3.

A log-log plot of the axial shear stress parameter $f''(1)$ *vs.* R is given in Figures 2(a,b) for selected values of S in the range $-4 \leqslant S \leqslant 4$. For $S > 0$, Figure 2(a) shows that $f''(1)$ increases with both R and S in agreement with the suction asymptotics $(22)_2$. The blowing results for $S < 0$ presented in Figure 2(b) show that all $f''(1)$ curves collapse onto the low Reynolds number $S = 0$ case solved numerically by Wang (1). At large values of R the numerical results tend smoothly to the asymptotic prediction (27), valid for $R|S| \gg 1$. It is

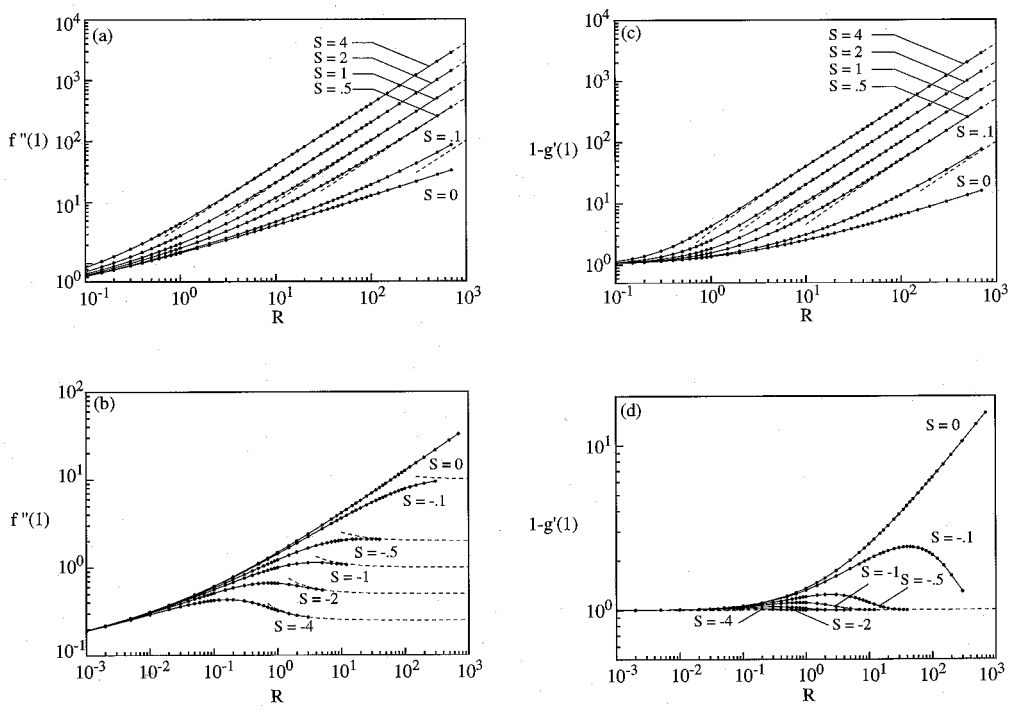

Figure 2. Numerically computed shear-stress parameters plotted on log-log scale as a function of R for selected values of S; axial shear-stress parameter for (a) suction and (b) blowing; azimuthal shear stress parameter for (c) suction, and (d) blowing. The dashed curves represent asymptotic behaviors given by Equations $(22)_2$ and $(23)_2$ for suction at large RS and by Equations (27) and (37) for blowing at large $R|S|$.

apparent that convergence occurs at much higher values of R as $|S|$ decreases toward zero. Moreover, for $R|S| \to \infty$, the leading behavior of $(37)_2$ is simply

$$f''(1) \sim \frac{1}{|S|}, \tag{41}$$

which matches very closely to the intercepts of the asymptotic (dashed) curves with the right hand ordinate in Figure 2(b).

Figures 2(c,d) exhibit log-log plots of $[1 - g'(1)]$ as a function of R for transpiration in the range $-4 \leqslant S \leqslant 4$. The results for suction plotted in Figure 2(c) converge to the asymptotic behavior given by $(23)_2$ in the same manner as the suction results for $f''(1)$, namely convergence at high values of S occurs at low values of R, and *vice versa*. The blowing results displayed in Figure 2(d) converge to the asymptotic limit (37) both as $|S| \to \infty$ for fixed R, and as $R \to \infty$ for fixed $|S|$. In fact, the numerical results for $S = -4$ indicate that for not much larger values of $|S|$, the azimuthal shear stress will be *independent* of the Reynolds number, and equal to its asymptotic value.

4.2. VELOCITY PROFILES

The axial and azimuthal velocity components given in (5) are proportional to $f'(\eta)$ and $\eta^{-1/2} g(\eta)$, respectively. Sample velocity profiles for suction and blowing are now presented

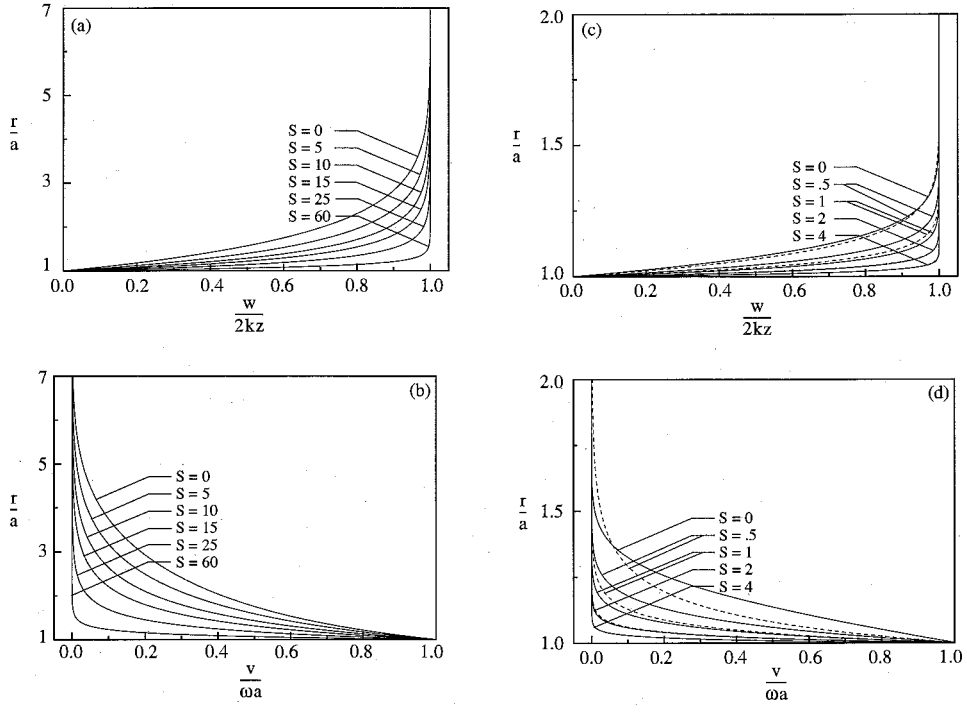

Figure 3. Sample suction velocity profiles; axial profiles (a) and azimuthal profiles (b) for $R = 0{\cdot}1$; axial profiles (c) and azimuthal profiles (d) for $R = 10$. The dashed profiles in (c) and (d) are asymptotic suction profiles given by Equations $(22)_1$ and $(23)_1$, respectively.

for $R = 0{\cdot}1$ and $R = 10$ representing typical small and large values of the stagnation flow Reynolds number, respectively.

With $S = 0$ and $\Omega = 0$, Wang [1] pointed out that a fixed stagnation circle exists on the cylinder at $z = 0$. With uniform blowing through a stationary porous cylinder, this circle expands outward to become a free stagnation circle residing in the surface $r/a = (\eta_c)^{1/2} \equiv \sigma$ of zero radial velocity. It should be borne in mind that, once $\Omega \neq 0$, the free stagnation circle becomes a circle of pure swirl owing to the finite azimuthal velocity induced everywhere in the fluid by the rotating cylinder. With uniform suction the stagnation circle is sucked into the porous cylinder, in which case there is no point of stagnation in the entire fluid.

Sample axial and azimuthal velocity profiles at $R = 0{\cdot}1$ are presented in Figures 3(a,b), respectively, for selected values of the suction parameter in the range $0 \leqslant S \leqslant 60$. Similar plots at $R = 10{\cdot}0$ covering the range $0 \leqslant S \leqslant 4$ are displayed in Figures 3(c,d). In Figure 3(d) we have included, as dashed lines for comparison, the asymptotic forms of the axial and azimuthal velocity distributions computed from Equations $(22)_1$ and $(23)_1$, respectively. Note that the numerical and asymptotic profiles are indistinguishable at $S = 4$ for this value of R. The value $RS = 20$ where the profiles come into essential agreement provides an estimate as to how large RS must be for the asymptotic results to be valid at other Reynolds numbers. Noting the change of ordinate scale for results given at $R = 0{\cdot}1$ and $R = 10{\cdot}0$, we observe that the thinning of the boundary layer with increasing values of both R and S is evident.

Sample blowing velocity profiles are given in Figure 4. In these figures dots denote the position $r/a = \sigma$ of zero radial velocity. The velocity profiles at $R = 0{\cdot}1$ displayed in Figures 4(a,b) for blowing parameters in the range $-25 \leqslant S \leqslant 0$ show the outward displacement

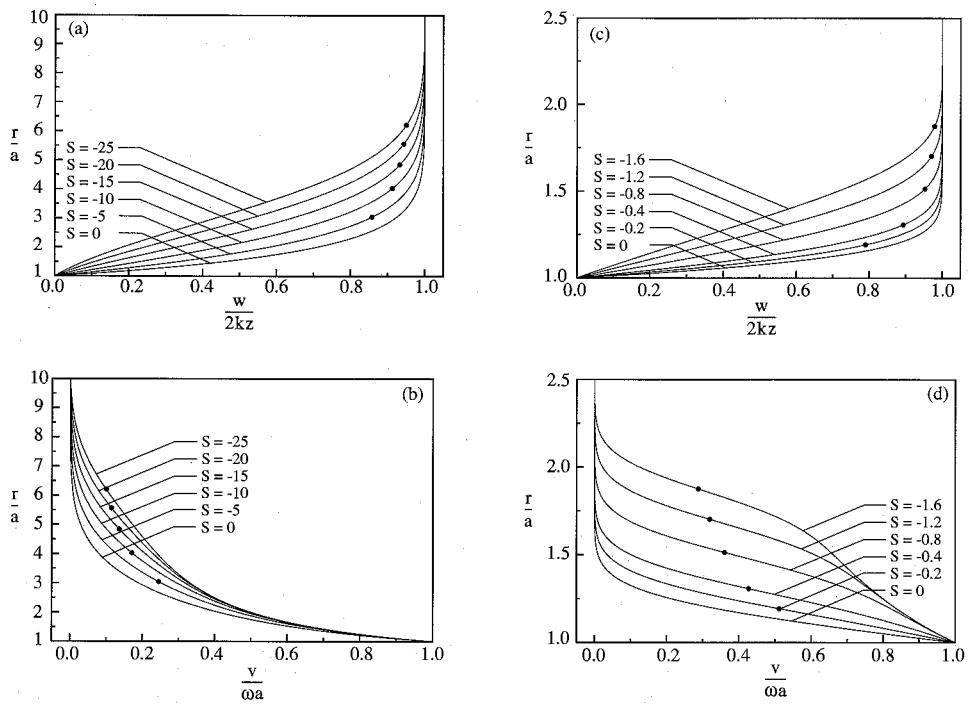

Figure 4. Sample blowing velocity profiles; axial profiles (a) and azimuthal profiles (b) for $R = 0{\cdot}1$; axial profiles (c) and azimuthal profiles (d) for $R = 10$. The dots denote the stand-off position of the stagnation circle.

of the zero radial velocity circle with increasing blowing strength. Note in Figure 4(b) that for all $S < -5$, the wall slopes of the dimensionless azimuthal velocity profiles have attained their limiting value $\mathrm{d}(v/\omega a)/\mathrm{d}(r/a) = -1$, in agreement with the Reynolds-number-independent result $g'(1) = 0$ in Figure 2(d) for $|S| \to \infty$. Velocity profiles at $R = 10$ over the range $-1.6 \leqslant S \leqslant 0$ are given in Figures 4(c,d). The same thickening of axial and azimuthal boundary layers with increasing blowing strength is observed as in the low Reynolds number results, but now a plateau centered on $r/a = \sigma$ appears in the azimuthal profiles at large values of $|S|$. This is consistent with the composite structure of the large blowing asymptotics found in Section 3.2. At the highest value of blowing in each of these figures we see the development of $(r/a)^{-1}$ behavior near the cylinder wall, the emergence of the viscous layer centered at $r/a = \sigma$ described by the error function in Equation (40), and the final exponential decay to zero velocity as $\eta \to \infty$.

4.3. Flow kinematics

Although axisymmetric, the flow field is fully three-dimensional. Particle-path lines may be found by superimposing the streamline flow in the meridional plane with the azimuthal flow at each value of R, S, and Ω. The kinematics of the motion for blowing and suction flows will now be illustrated. The dimensionless meridional streamline field given by Equation (18) for a suction flow with $R = 1$, $S = 1$, and $\Omega = 40$ is displayed in Figure 5(a). Notice that all streamlines enter the cylinder normally in the meridional plane, as required by the boundary conditions. Projected pathlines, depicting the three-dimensional nature of the flow, corresponding to stremlines $\hat{\psi} = 0{\cdot}2, 2{\cdot}0$ and $20{\cdot}0$ are shown in Figure 5(b). The pathlines

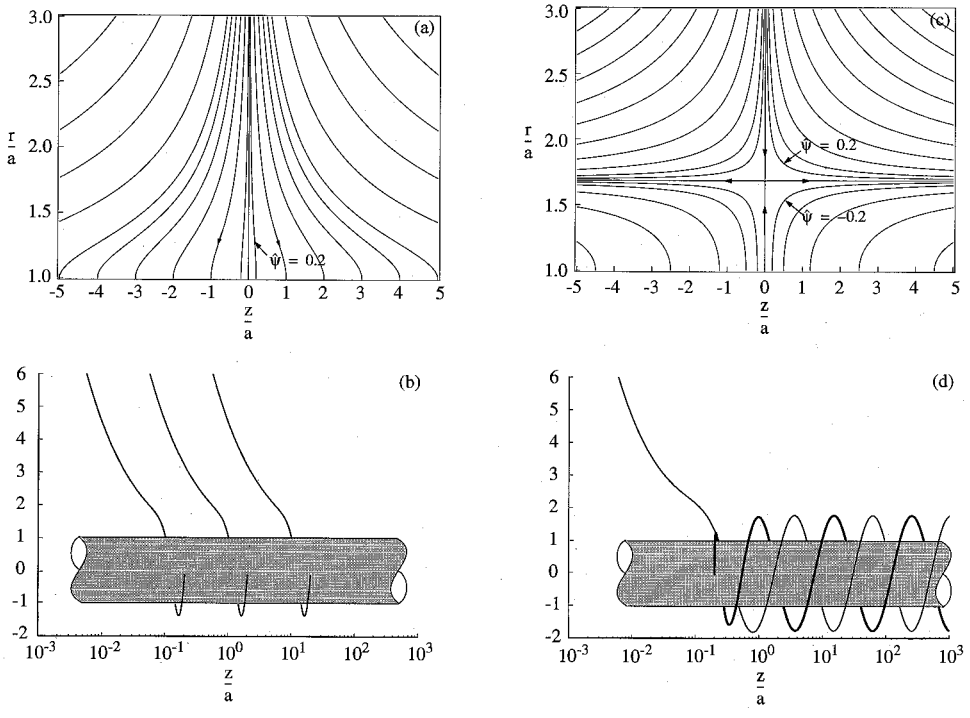

Figure 5. Suction streamlines (a) computed at $R = 1$ and $S = 1$ and (b) corresponding pathlines computed at $\Omega = 40$ for $\hat{\psi} = 0{\cdot}2, 2{\cdot}0, 20{\cdot}0$. Blowing streamlines (c) computed at $R = 1$ and $S = -1$ and (d) corresponding pathlines computed at $\Omega = 40$ for $\hat{\psi} = \pm 0{\cdot}2$. The stand-off distance to the cylinder of zero radial velocity is $r/a = 1{\cdot}685$.

approach the cylinder radially from infinity, wind around the cylinder, and ultimately enter the porous cylinder wall. Since $f(1) = S$, it may be readily shown from (18) that the axial position z/a at which a particle leaves the cylinder in the case of blowing, or enters the cylinder in the case of suction, is given by $\hat{\psi}/S$. Thus the particles enter the cylinder at $z/a = 0{\cdot}2, 2{\cdot}0$ and $20{\cdot}0$ in Figure 5(b).

Figure 5(c) shows the meridional streamlines for a blowing flow with $R = 1$, $S = -1$, and $\Omega = 20$. The outward transpiration from the cylinder stops the radially inward stagnation flow at $r/a = \sigma = 1{\cdot}685$, where $\hat{\psi} = 0$. Figure 5(d) shows two pathlines; one corresponds to the interior streamline $\hat{\psi} = -0{\cdot}2$ and the other to the exterior streamline $\hat{\psi} = 0{\cdot}2$, both labeled in Figure 5(c). Outside the boundary layer the thin pathline approaching the cylinder from above follows a trajectory similar to those in Figure 5(b). Once it enters the boundary layer of the azimuthal flow it picks up a swirl component of velocity and spirals around the cylinder. The bold pathline leaving the cylinder at $z/a = 0{\cdot}2$ moves radially outward as it rotates in the flow of the azimuthal boundary layer. These interior pathlines converge rapidly to the surface $r/a = \sigma$ of zero radial velocity. Indeed, all particles approaching from infinity and all particles passing through the cylinder wall tend to the zero radial velocity surface as $z \to \pm\infty$, and hence the circles $r/a = \sigma$ at positive and negative infinity may be considered as 'attractors' for the flow.

Other descriptors of the kinematics, such as the local spiral flow angle in the $r - \theta$ plane, the local helical flow angle in the $r - z$ plane, and the flow helicity (Moffatt [12]) have

been computed by Cunning [13]. There it is shown that the helicity is everywhere finite for suction flows, while for zero transpiration and blowing flows the helicity becomes infinite as $z \to \pm\infty$.

5. Discussion and conclusion

We have investigated the effects of cylinder rotation and transpiration on radial stagnation flow, using both numerical integration and asymptotic analysis. A coordinate separation of the velocity and pressure fields reduces the Navier-Stokes equations to a *primary* nonlinear equation for the meridional flow and a coupled linear *secondary* equation for the azimuthal flow. Numerical solutions are obtained over a range of stagnation-flow Reynolds numbers R and dimensionless transpiration numbers S. The computed shear-stress parameters approach the asymptotic behaviors found for $RS \gg 1$ in the case of suction and for $R|S| \gg 1$ for blowing. The fact that all numerical solutions blend accurately onto the asymptotic results provides a validation of the numerical results; this is a particularly rigorous test of the numerics since the asymptotic regions of the flow coincide with the R-S parameter space regime where the equations become increasingly stiff.

The velocity profiles for blowing have interesting structures. Each set of axial velocity profiles at fixed R shows that the surface $r/a = \sigma$ of zero radial velocity moves ever closer to the outer edge of the boundary layer as blowing increases. The numerics show that this surface is also the center of a cylindrical free shear layer that develops in the azimuthal flow at large values of $|S|$. The free shear layer is always connected to a wall boundary layer which has the distinct feature that its shear-stress parameter $g'(1) = 0$ is Reynolds-number-independent as $|S| \to \infty$. The essential mathematical description of the structure of these boundary layers is encompassed in the large $R|S|$ asymptotic analysis given in Section 3.2. There we have shown that the axial boundary layer simply thickens with increasing blowing; the swirling flow, on the other hand, develops into a separated circular free shear layer with error-function behavior of thickness $O[a(R|S|)^{-1/2}]$ centered on $r/a = \sigma$, connected to an ever present wall viscous layer.

Blown-off boundary layers that evolve into free shear layers have been identified previously. The separation of a Blasius boundary layer by injection through the surface of a flat plate was the subject of studies by Kassoy [14], Klemp and Acrivos [15], and others. The separated viscous shear layer in this case follows a parabolic trajectory emanating from the leading edge of the plate. More akin to the present problem is the study by Kuiken [16] on the separation, by strong normal blowing, of the Kármán boundary-layer formed on an infinite disk rotating beneath a quiescent fluid. Here, the swirling boundary layer flow is blown away to form a thin flat viscous layer standing above an inviscid region of uniform depth, analogous to the uniform radial stand-off distance $r/a = \sigma$ in the present problem. Direct injection is not the only manner by which boundary layers may be blown away. For example, Riley and Weidman [17] analyzed the structure of the boundary layer formed on a flat plate moving into its leading edge origin with constant speed, opposite to that of the uniform mainstream. In that problem, the boundary layer is forced away from the wall to form a free shear layer with no remnant of the wall boundary layer left behind. When uniform cross-flow is superposed, Weidman [18] found that both the primary (streamwise) flow and the secondary (cross-flow) blow off *simultaneously*, an evident fact that the secondary flow is slaved to the primary flow.

The thickening of the axial boundary layer with increased blowing against radial flow stagnating on a circular cylinder is consistent with the effects of injection in generalized

three-dimensional flows stagnating on a flat surface. Libby [20], among others, has shown that Hiemenz, Homann, and the generalized Howarth [21] stagnation-flow boundary layers simply thicken with increasing injection of the same fluid. Massive injection of a different miscible fluid, on the other hand, does produce a thin viscous free shear layer across which the fluid composition also changes. The unexpected development of a separated circular shear layer in the swirling flow, not slaved to a blown-off shear layer in the primary flow, deserves special attention. The free shear layer owes its existence to a change of sign in the inertia term in Equation (7) which is wrought by the sign change in radial velocity at $r/a = \sigma$. Thus, the development of the circular free shear layer is still directly linked to the stagnation flow, even though the latter does not itself exhibit a blown-off shear layer.

The axial velocity profiles show that at fixed R the boundary layer thickness decreases (increases) with increasing suction (blowing). We quantify this result by calculating the displacement thickness δ^* produced by the viscous axial flow, defined as the defficiency in axial mass flux in the viscous boundary layer relative to the inviscid axial mass flux. Mathematically, the relation is

$$\rho w_\infty(z)\pi[(\delta^* + a)^2 - a^2] = 2\pi \int_a^\infty \rho[w_\infty(z) - w(r,z)]r \, \mathrm{d}r, \tag{42}$$

where $w_\infty(z)$ is the axial component of the inviscid flow given in (3) and $w(r,z)$ is the viscous counterpart given in (5). Converting to the η-coordinate, we find

$$\hat{\delta}^*(\hat{\delta}^* + 2) = \int_1^\infty [1 - f'(\eta)] \, \mathrm{d}\eta, \tag{43}$$

where $\hat{\delta}^* = \delta/a$. Carrying out the integration, we find that the normalized displacement thickness for the axial flow is governed by the quadratic equation

$$(\hat{\delta}^*)^2 + 2\hat{\delta}^* + (1 - S - \lambda) = 0, \tag{44}$$

where

$$\lambda = \lim_{\eta\to\infty}[\eta - f(\eta)]. \tag{45}$$

For suction with $RS \gg 1$, the asymptotic behavior of $f(\eta)$ uniformly valid in η is given by (21). Using this equation, we readily find the limit (45) to be

$$\lambda = -(S-1) + \frac{1}{RS} \quad (RS \gg 1), \tag{46}$$

and solution of (44), choosing the physically relevant (positive) root, furnishes the asymptotic behavior for the displacement thickness

$$\hat{\delta}^* = \frac{1}{2}\frac{1}{RS} \quad (RS \gg 1). \tag{47}$$

For blowing with $R|S| \gg 1$, the analysis in Section 3.2 gives the approximate asymptotic result

$$\hat{\delta}^* = D - 1 \quad (R|S| \gg 1), \tag{48}$$

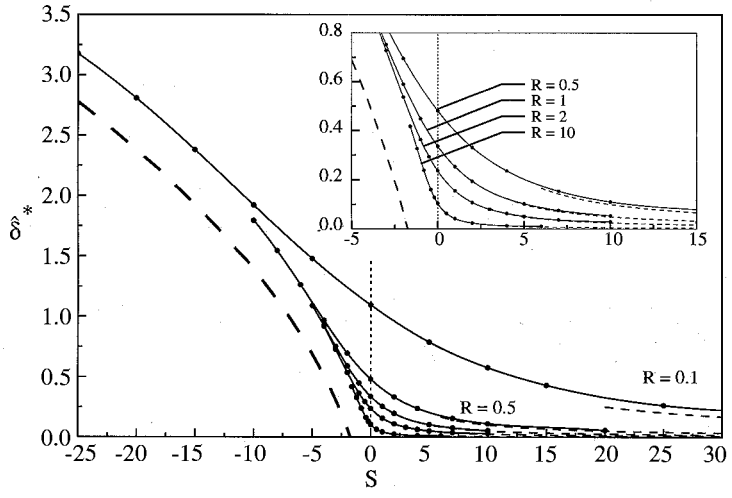

Figure 6. Plot of the nondimensional axial boundary-layer displacement thickness as a function of transpiration S for selected values of R. The dashed lines are asymptotic results given by Equation (47) for suction and Equation (48) for blowing.

where $D = D(R, S)$ appears in (36). This analytic result is only approximate because the term $\eta f'''$ in (6) was neglected. A proper representation for $\hat{\delta}^*$ at large blowing, asymptotic or exact, can only be obtained by direct numerical integration of the full governing equation.

Figure 6 compares asymptotic suction and blowing results with values of $\hat{\delta}^*$ computed from Equation (44) using eaxct numerical results to find λ for a range of values of S at $R = 0.1, 0.5, 1$ and 10. We can clearly see that increasing the blowing at fixed R increases the displacement thickness, and *vice versa*. The bold dashed line is a plot of the approximate asymptotic behavior given in (48) for $R \to \infty$, showing independence of $\hat{\delta}^*$ on R in this limit, in agreement with the numerical results. However, the approximate large blowing asymptotic prediction is somewhat smaller than the exact numerical results for $\hat{\delta}^*$. For suction with $S > 0$, the decrease in displacement thickness is seen to converge to the asymptotic prediction (47) rather quickly, in the neighborhood $RS \sim 5$.

To summarize, an exact separable solution to the Navier-Stokes equations for exterior radial stagnation flow approaching a rotating cylinder with uniform transpiration is presented. The parameter space R and S of solutions is covered completely by a combination of numerical integrations and asymptotic analysis. An interesting development is observed at large values of blowing where a cylindrical free shear layer separates out from the attached wall layer. We note in closing that the problem of radial stagnation flow *interior* to a cylinder, formed by blowing through the surface of a smaller concentric cylinder or from a line source coincident with the cylinder axis, has been reported recently by Marquès, *et al.* [19].

Acknowledgement

This work was completed while author PDW was on sabbatical leave. He extends his gratitude to École Polytechnique for supporting a six-month visit to the Laboratoire d'Hydrodynamique in Palaiseau, France and to the Spanish Ministry of Education and Culture for a three month visit to Escuela Técnica Superior de Ingenieros Aeronáuticos in Madrid, Spain under contract number SAB95-0514.

References

1. C.-Y. Wang, Axisymmetric stagnation flow on a cylinder. *Q. Appl. Math.* 32 (1974) 207–213.
2. C.-Y. Wang, Exact solutions of the steady-state Navier-Stokes equations. In: J. L. Lumley, M. Van Dyke, H. L. Reed (eds.) *Ann. Rev. Fluid Mech.* Palo Alto: Annual Reviews Incorporated 23 (1991) pp. 159–177.
3. R. S. R. Gorla, Nonsimilar axisymmetric stagnation flow on a moving cylinder. *Int. J. Eng. Sci.* 16 (1978) 392–400.
4. R. S. R. Gorla, Unsteady viscous flow in the vicinity of an axisymmetric stagnation point on a circular cylinder. *Int. J. Eng. Sci.* 17 (1979) 87–93.
5. R. S. R. Gorla, Transient response behavior of an axisymmetric stagnation flow on a circular cylinder due to a time dependent free stream velocity. *Lett. Appl. Eng. Sci.* 16 (1978) 493–502.
6. K. Hiemenz, Die Grenzschicht an einem in den gleichförmingen Flussigkeitsstrom eingetauchten geraden Kreiszylinder. *Dinglers Polytech. J.* 326 (1911) 321–410.
7. F. Homann, Der Einfluss grosser Zähighkeit bei der Strömung um den Zylinder und um die Kugel. *Zeitsch. Angew. Math. Mech.* 16 (1936) 153–164.
8. F. S. Sherman, *Viscous Flow*. New York: McGraw-Hill (1990) 746 pp.
9. W. H. Press, B. P. Flannery, S. A. Teukolsky and W. T. Vetterling, *Numerical Recipes*, 2*nd* edition. Cambridge: Cambridge University Press (1992) 963 pp.
10. J. Pretsch, Grenzen der Grenzschichtbeeinflussung. *Zeitsch. Angew. Math. Mech.* 24 (1944) 264–267.
11. L. Rosenhead, *Laminar Boundary Layers*. Oxford: Oxford University Press (1963) 688 pp.
12. H. K. Moffatt, The degree of knottedness of tangled vortex lines. *J. Fluid Mech.* 35 (1969) 117–129.
13. G. M. Cunning, Axisymmetric stagnation point flow on a rotating circular cylinder with uniform transpiration. Masters of Science Thesis, University of Colorado, Boulder, Colorado, USA (1995) 57 pp.
14. D. R. Kassoy, On laminar boundary layer blowoff. *SIAM J. Appl. Math.* 49 (1970) 29–40.
15. J. B. Klemp and A. Acrivos, High Reynolds number flow past a flat plate with strong blowing. *J. Fluid Mech.* 51 (1972) 337–356.
16. H. K. Kuiken, The effect of normal blowing on the flow near a rotating disk of infinite extent. *J. Fluid Mech.* 47 (1971) 789–798.
17. N. Riley and P. D. Weidman, Multiple solutions of the Falkner-Skan equation for flow past a stretching boundary. *SIAM J. Appl. Math.* 49 (1989) 1350–1358.
18. P. D. Weidman, New solutions for laminar boundary layers with cross flow. *Zeitsch. Angew. Math. Phys.* 48 (1997) 341–356.
19. F. Marquès, J. Sánchez, and P. D. Weidman, A generalized Couette-Poiseuille flow with boundary mass transfer. Submitted to *J. Fluid Mech*.
20. P. A. Libby, Laminar flow at a three-dimensional stagnation point with large rates of injection. *Am. Inst. Aeron. Astr. J.* 14 (1976) 1273–1279.
21. L. Howarth, The boundary layer in three dimensional flow. Part II. The flow near a stagnation point. *Phil. Mag.* Series 7, 42 (1951) 1433–1440.